Article

Not peer-reviewed version

Photo- and X-ray Induced Cytotoxicity of CeF_3-YF_3-TbF_3 Nano-Particle-Polyvinylpyrrolidone –"Radachlorin" Composites for Combined Photodynamic Therapy

Alina Khusainova , Alexey Nizamutdinov * , Nail Shamsutdinov , Svetlana Kalinichenko , Damir Safin , Marat Gafurov * , Elena Lukinova , Sergey Batygov , Sergey Kuznetsov , Sergey Zinchenko , Pavel Zelenikhin , Maksim Pudovkin

Posted Date: 16 November 2023

doi: 10.20944/preprints202311.1050.v1

Keywords: Photodynamic therapy; combined photodynamic therapy; Radachlorin; nanoparticle-photosensitizer conjugates

Article

Photo- and X-ray Induced Cytotoxicity of CeF_3-YF_3-TbF_3 Nanoparticle- Polyvinylpyrrolidone – "Radachlorin" Composites for Combined Photodynamic Therapy

Alina I. Khusainova [1], Alexey S. Nizamutdinov [1,*], Nail I. Shamsutdinov [1], Svetlana Kalinichenko [1], Damir I. Safin [1], Marat Gafurov [1,*], Elena V. Lukinova [2], Sergey Kh. Batygov [3], Sergey V. Kuznetsov [3], Sergey V. Zinchenko [1], Pavel V. Zelenikhin [1] and Maksim Pudovkin [1]

[1] Kazan Federal University, 18 Kremlyovskaya str, Kazan, 420008, Russian Federation;
[2] Belgorod State National Research University, 85 Pobedy Str., 308015 Belgorod, Russia
[3] Prokhorov General Physics Institute of the Russian Academy of Sciences, Moscow, Russia
* Correspondence: *A. Nizamutdinov. anizamutdinov@mail.ru

Abstract: The $Ce_{0.5}Y_{0.35}Tb_{0.15}F_3$ nanoparticles with CeF_3 hexagonal structure were synthesized by co-precipitation technique. The average nanoparticle diameter was 14±1 nm. The luminescence decay curves of $Ce_{0.5}Y_{0.35}Tb_{0.15}F_3$ nanoparticles (λ_{em} = 541 nm, $^5D_4$ – $^7F_5$ transition of Tb^{3+}) conjugated with Radachlorin by means of polyvinylpyrrolidone coating as well as without Radachlorin were detected. Efficient nonradiative energy transfer from Tb^{3+} to the Radachlorin was demonstrated. The maximum energy transfer coefficient for nanoparticles conjugated with Radachlorin via polyvinylpyrrolidone and without the coating were 82% and 55%, respectively. The average distance between nanoparticle surface and Radachlorin was R_0 =4.5 nm. The best results for X-ray induced cytotoxicity was observed for NP-PVP-Rch sample at the lowest Rch concentration. In particular, after X-ray irradiation the survival A 549 human lung carcinoma cells decreased by ~12%.

Keywords: photodynamic therapy; combined photodynamic therapy; Radachlorin; nanoparticle-photosensitizer conjugates

1. Introduction

For many years, mankind has been developing the oncological diseases therapies. One of the promising methods is a photodynamic therapy (PDT), which is based on the activation of photosensitizer molecules via visible light [1–4]. In particular, photosensitizer molecules can accumulate in the tumor and being exposed to laser radiation the photosensitizer molecule receives energy and transfers it to the oxygen and water molecules, turning it into excited states (so-called reactive oxygen species). The singlet oxygen can be classified as reactive oxygen species that are highly aggressive oxidizer. As a consequence, these forms of oxygen can damage the vascular system of the tumor through cell necrosis or apoptosis [1,2]. However, the visible radiation is not able to penetrate into the tissues deeper than several centimeters [5]. Moreover, its power density sharply attenuates due to the several physical processes including scattering, reflection, and absorption [6], [7]. For these reasons, the use of PDT is limited and it can be used for treatment superficial tumors only. One of the ways to eliminate this problem is the use of method of combined PDT and ionizing irradiation therapies. This kind of electromagnetic waves can travel in the biological tissues with minimal losses.

The main idea of this method is that the photosensitizer molecules are bound to the scintillating nanoparticle. The absorption spectrum of the photosensitizer should overlap with the emission spectrum of the nanoparticle. Further, the energy of ionizing radiation is converted into the production of singlet oxygen.

 doi:10.20944/preprints202311.1050.v1

Very important requirements are imposed on the scintillating nanoparticles. Specifically, these nanoparticles should efficiently absorb ionizing radiation and convert its energy into photosensitizer excitation with subsequent formation of singlet oxygen.

Among a relatively big variety of scintillating materials, rare-earth fluoride nanoparticles are considered very promising for scintillating. Indeed, the presence of rare-earth element having high atomic number significantly increases the absorption cross-section. According to the literature data, fluoride nanoparticles can be easily coated with biocompatible polymers and loaded with photosensitizer. The coated and unmodified rare-earth fluoride nanoparticles demonstrate low cytotoxicity toward many cell lines [8–11]. Materials containing cerium are considered very efficient scintillators converting ionizing irradiation into UV one [12]. In its turn, the co-activation with Tb^{3+} ions allows obtaining intense green luminescence due to an effective energy transfer from Ce^{3+} to Tb^{3+} [13–15]. In this system, the brightest Tb^{3+} luminescence peaks correspond to $^5D_4 - {}^7F_J$ (J = 3 – 6) transitions. The Tb^{3+} luminescence overlaps with the absorption of one of some clinically approved photosensitizers based on chorine [16]. For the efficient X-ray induced PDT the conjugation method of photosensitizers and nanoparticles is crucial. In the case of inorganic photosensitizers such as ZnO, it is possible to create a double phase nanocomposites [17], [18] or core-shell structure [19]. For clinically approved organic photosensitizers a polymeric shell is required in many cases. In particular, polyethylenimine (PIE) on the surface of $Cu_{2-x}S$ nanoparticles can be branched with chlorin (e6) [20]. Also the possibility of Chlorin e6-based photosensitizer conjugation to Polyvinylpyrrolidone (PVP) has been shown in several works [21–24].

However, the work demonstrates conjugation of Tb^{3+}:LaF_3 nanoparticles with Rose Bengal via electrostatic interaction of negatively charger functional groups of Rose Bengal photosensitizer and positively charged Tb^{3+}:LaF_3 nanoparticle surface due to F^- vacancies on the surface. In its turn, the Eu^{3+}:$BaGdF_5/SiO_2$ core/shell nanoparticles loaded with methylene blue photosensitizer demonstrated their efficiency in X-ray induced PDT due to the porous nature of SiO_2 shell [25].

The search of convenient coating polymers for conjugation with specific photosensitizers is a very challenging task in modern scientific community.

In our previous work [16], we demonstrated the efficiency of energy transfer from CeF_3-YF_3-TbF_3 nanoparticles to Radachlorin via PVP. The aim of this work was to study the spectral and kinetic characteristics of promising nanocomposites based on $Ce_{0.5}Y_{0.35}Tb_{0.15}F_3$ nanoparticles conjugated with Radachlorin by means of polyvinylpyrrolidone. The nonradiative energy transfer from Tb^{3+} ions to Radachlorin molecules was investigated. The toxicity of the composites to the A549 cell culture was also evaluated using the MTT test.

2. Materials and Methods

2.1. Experimental technique

The optical excitation of the luminescence was performed via 266 nm laser radiation, the 4th harmonic of YAG:Nd laser from Lotis TII LS-2147, which operated in Q-switched mode (pulse duration was 10 ns). The spectra were registered using StellarNet portable spectrometer. The luminescence decay curves we registered by monochromator with 1200 lines per mm diffraction grating. The signal was registered by means of photomultiplier tube FEU100 and digital oscilloscope Rhode&Schwartz with 1 GHz bandwidth. The X-ray luminescence (XRL) spectra of the prepared samples were measured on a laboratory installation built of an X-ray source (tungsten anode operating at a voltage of 40 kV and a current of 35 mA) and an FSD-10 mini-spectrometer (Optofiber LLC, Moscow, Russia). Photodynamic activity of both Radachlorin and Radachlorin - CeF_3-YF_3-TbF_3 nanoparticle conjugated was studied using commercial medical light source based on laser emitting diode Latus (λ_{em} = 662 nm). Physical characterization of nanoparticles was performed with Bruker D8 diffractometer with Cu K_α-radiation and Hitachi HT7700 Exalens transmission electron microscope TEM) with accelerating voltage of 100 kV in TEM mode. The sample preparation: the suspension (10 microliters) was placed on a formvar/carbon lacey 3 mm copper grid; drying was performed at room temperature. After drying, the grid was placed in a transmission electron microscope using a special

 doi:10.20944/preprints202311.1050.v1

holder for microanalysis. The analysis was held at an accelerating voltage of 100 kV in TEM mode. The average diameter of the nanoparticles was estimated from the TEM images using the ImageJ software. Statistics are based on the analysis of 160 nanoparticles. Histogram plots were obtained with the OriginPro software. To get the diameter (D) of the nanoparticles, the area (in squire nanometers) of each nanoparticle from TEM image was equated to the area of a circle $\pi \cdot D^2/4$, where $\pi = 3.14$, and D is the diameter. The obtained histogram was approximated via Lognornal function where ±1 standard deviation was determined.

2.2. Synthesis of the nanoparticles

The CeF_3-YF_3-TbF_3 nanoparticles were fabricated by co-precipitation from aqueous solution technique. It is well established synthesis which result in nanoparticles of good crystallinity and relatively small dimensions for CeF_3 based compounds [26]. We used an ammonium citrate solution with a 3-fold excess of NH_4F as fluorinating agent. All the chemicals used are of analytical grade. Monohydrate citric acid ($C_6H_8O_7 \cdot H_2O$), $Y(NO_3)_3 \cdot 6H_2O$, $Ce(NO_3)_3 \cdot 6H_2O$, $Tb(NO_3)_3 \cdot 6H_2O$, NH_4F, ammonium, polyvinylpyrrolidone (PVP) were purchased from Sigma – Aldrich. All the chemicals were used without further purification. The concentration of the doping ions is represented in molar percentage (mol.%). The choice of $Ce_{0.5}Y_{0.35}Tb_{0.15}F_3$ sample was based on the observation, that at these ratios between the ions the highest energy transfer rate from Ce^{3+} to Tb^{3+} occurs [27], [28]. In order to form PVP-nanoparticle composites, 100 mg of dried nanoparticles were suspended in 10 mL of distilled water via sonication. Also, 25 ml of distilled water was added to 100 mg of PVP. The mixture was placed to ultrasonic bath (model ODALQ40, 600 W, volume 4 L) for 7 min in order to obtain homogenous solution. The colloidal solution of the nanoparticles was added dropwise to PVP solution and stirred for several hours. Washing by centrifugation was carried out to remove residual unreacted PVP (until pH factor was about 6). A solution of polyvinylpyrrolidone with a mass fraction of 1% was added dropwise to the colloid of nanoparticles with continuous stirring. We used commercially available Radachlorin as photosensitizer produced by RadaPharma company. It consists of 3,5 mg/ml water solution of mixture of sodium salts of chlorine e6, chlorine p6 and purpurin 5 [29].

3. Results

3.1. Characterization of $Ce_{0.5}Y_{0.35}Tb_{0.15}F_3$ nanoparticles

The X-ray diffraction pattern of $Ce_{0.5}Y_{0.35}Tb_{0.15}F_3$ powder is presented in Figure 1.

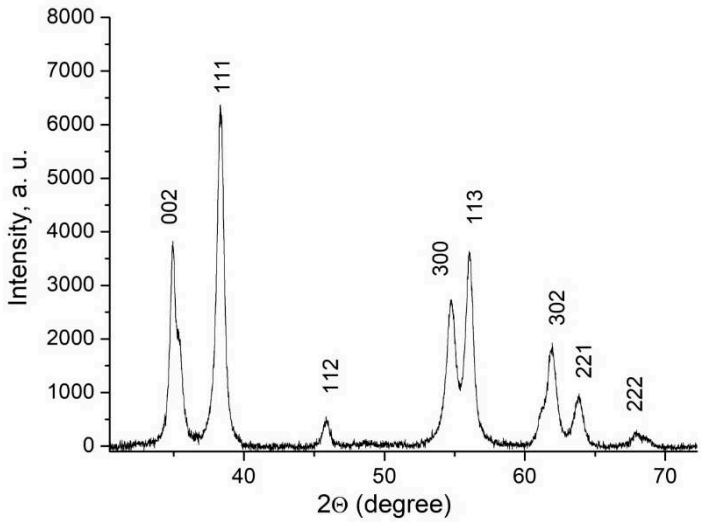

Figure 1. X-ray diffraction pattern of $Ce_{0.5}Y_{0.35}Tb_{0.15}F_3$ nanoparticles.

Preprints (www.preprints.org) | NOT PEER-REVIEWED | Posted: 16 November 2023 doi:10.20944/preprints202311.1050.v1

The obtained pattern corresponds to the hexagonal structure of CeF_3 host-matrix. The crystal lattice parameters of the samples were determined, namely a = 7.02 ± 0.15 Å , c = 7.20 ± 0.14 Å [30]. TEM image of the nanoparticles and the size distribution histogram are presented in Figure 2a and b, respectively.

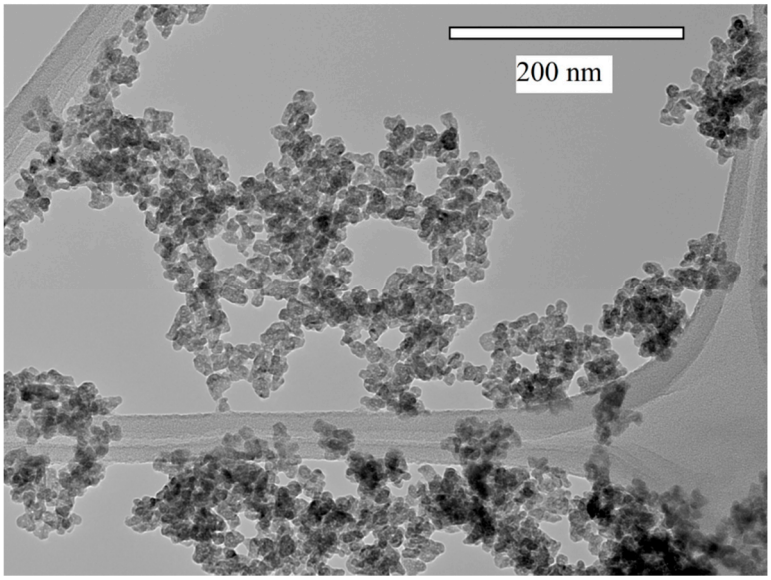

(a)

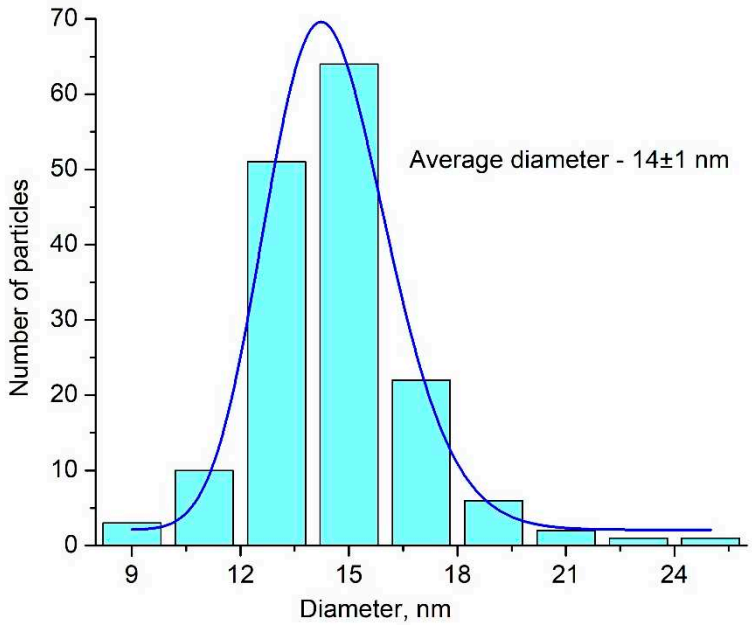

(b)

Figure 2. TEM image (a) and the size distribution histogram (b) of $Ce_{0.5}Y_{0.35}Tb_{0.15}F_3$ nanoparticles

The nanoparticles morphology is not perfectly regular with average diameter around 14±1 nm. Nanoparticles with this size without agglomerations can be used for biomedical applications [1].

3.2. Spectral-kinetic characteristics of nanoparticles $Ce_{0.5}Y_{0.35}Tb_{0.15}F_3$

Preprints (www.preprints.org) | NOT PEER-REVIEWED | Posted: 16 November 2023 doi:10.20944/preprints202311.1050.v1

The luminescence spectrum of 7.9 g/L water colloidal solution ($Ce_{0.5}Y_{0.35}Tb_{0.15}F_3$ nanoparticles) under 266 nm excitation is shown in Figure 3.

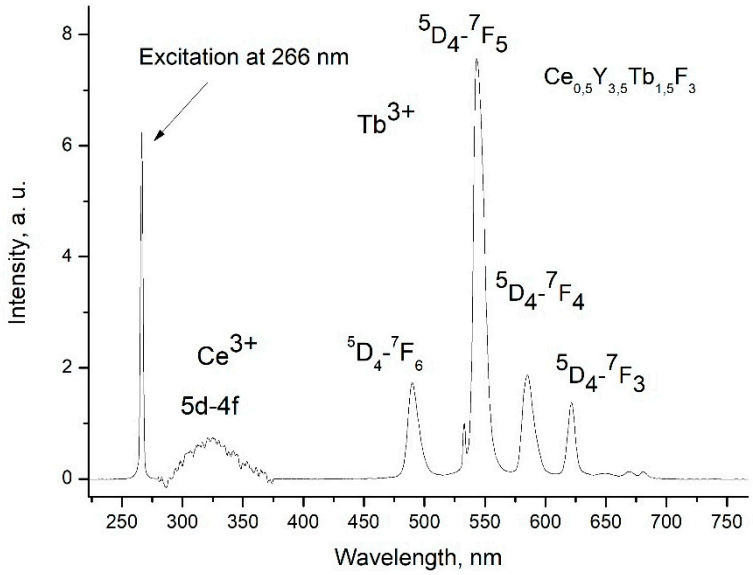

Figure 3. Room temperature luminescence spectra of $Ce_{0.5}Y_{0.35}Tb_{0.15}F_3$ nanoparticles as 7.9 g/L water colloidal solution. λ_{ex} = 266 nm corresponds to 4f – 5d absorption band of Ce^{3+}.

The luminescence peaks correspond to trivalent terbium and cerium ions. Specifically, the broad luminescence band in the 280 – 400 nm spectral range is due to the 5d – 4f transitions of Ce^{3+} ions. It its turn, the peaks in the visible spectral range are 4f – 4f emissions of Tb^{3+} ions (transitions from $^5D_4$ to ^7F_J). The possibility of nanoparticle conjugation with photosensitizer molecules was studied using polyvinylpyrrolidone (PVP) as coating material of the nanoparticles. The Radachlorin (Rch) photosensitizer was diluted in distilled water in a ratio of 6:50 (0.5 ml of water and 60 μl of Radochlorin) and added in different volumes to the colloidal solutions of nanoparticles coated with PVP and without the coating (two samples). The luminescence kinetics of Tb^{3+} ions (λ_{em} = 541 nm, $^5D_4$ – $^7F_5$ transition) of PVP- coated nanoparticles (a) and unmodified ones (b), decay times at different Radachlorine concentrations (c), and energy transfer coefficients (d) are presented at Figure 4.

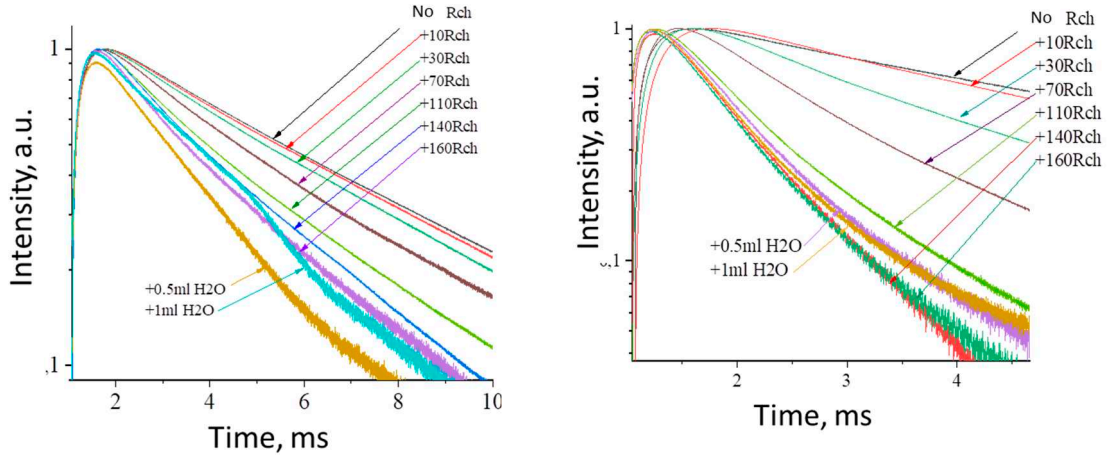

(a) **(b)**

Preprints (www.preprints.org) | NOT PEER-REVIEWED | Posted: 16 November 2023 doi:10.20944/preprints202311.1050.v1

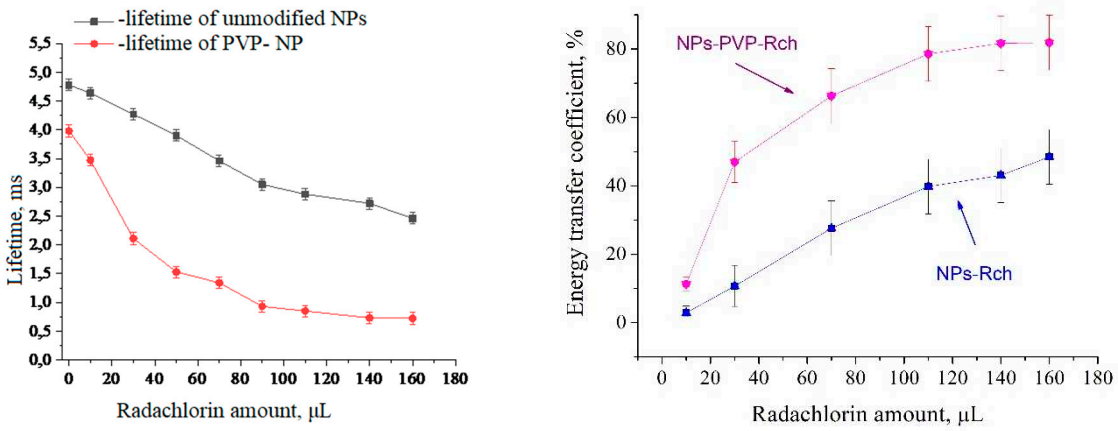

(c) (d)

Figure 4. The luminescence kinetics of Tb^{3+} ions (λ_{em} = 541 nm, $^5D_4$ – $^7F_5$ transition) of PVP- coated nanoparticles (a) and unmodified ones (b), decay times at different Rch concentrations (c), and energy transfer coefficients (d).

It can be seen, that an increase in the concentration of Rch molecules in the colloid leads to the shortening of the luminescence decay times of Tb^{3+} ions which is apparently a consequence of efficient nonradiative energy transfer from nanoparticles to Rch. This tendency is observed for both types the samples (Figure 4a,b). We have diluted colloids with high concentration of Rch with distilled water to check the stability of the nanoparticle-Rch complexes. In the case of unmodified nanoparticles, the luminescence decay rate got back to the larger values. It means that this complex is not stable, and the photosensitizer molecules are capable of separating from the nanoparticle surface. In the case of nanoparticle-PVP-Rch composites, the decay curves stayed constant after the adding of water. It apparently indicates the formation of relatively stable conjugates. For higher concentrations of Rch, the deviation from single exponential law of the decay curves is observed. This observation can be related to the fact, that different nanoparticles are conjugated with different amounts of Rch molecules. In this case, the rate of Tb^{3+} luminescence quenching depends on the amount of conjugated Rch molecules, in its turn; it leads to the multiexponential character of the decay curve. The luminescence lifetime was calculated as an average lifetime according to the formula 1 [31]:

$$t_{av} = \frac{\int t * I(t)\, dt}{\int I(t)\, dt} \quad (1)$$

where $I(t)$ – is the luminescence intensity. The results of lifetime evaluation are presented at Figure 4c. The values of luminescence lifetime of Tb^{3+} ions at 541 nm obtained here for colloidal solution of unmodified nanoparticles without Rch appear to be larger than that obtained by us for dry samples in our previous work [15]. It can be explained by the radiative energy transfer between nanoparticles in colloid. The efficiency of energy transfer (k_{ET}) can be calculated from luminescence decay time values according to formula 2 [32]:

$$k_{ET} = 1 - {}^{\tau_{NPs}}/_{\tau_{NPs+Rch}} \quad (2)$$

where τ_{NPs} is the lifetime of $^5D_4$ – $^7F_5$ transition of Tb^{3+} ions in the absence of Rch and $\tau_{NPs+Rch}$ is the decay time of the same conjugated with Rch. The results of energy transfer coefficient evaluation are presented in Figure 4d. The efficiency of energy transfer for PVP coated nanoparticles increases faster at low amounts of Rch compared to unmodified nanoparticles. The highest value of energy transfer efficiency is 80 % in the solution with 140 - 160 µl Rch. It is possible to estimate the effective distance between Tb^{3+} ions and Rch molecules. The Forster resonance energy transfer (FRET) theory is a reliable approach for estimation of this value [33], [34]. The FRET is a strongly distance-dependent process of energy transfer between two elements (donor and acceptor). This energy transfer takes

Preprints (www.preprints.org) | NOT PEER-REVIEWED | Posted: 16 November 2023 doi:10.20944/preprints202311.1050.v1

place at a distance in the 1–20 nm range. For FRET, it is important, that the donor should be an emissive molecule or particle and acceptor should be able to absorb the light which donor emits. Radachlorin absorption spectrum and X-ray luminescence spectrum of $Ce_{0.5}Y_{0.35}Tb_{0.15}F_3$ nanoparticles are presented in Figure 5.

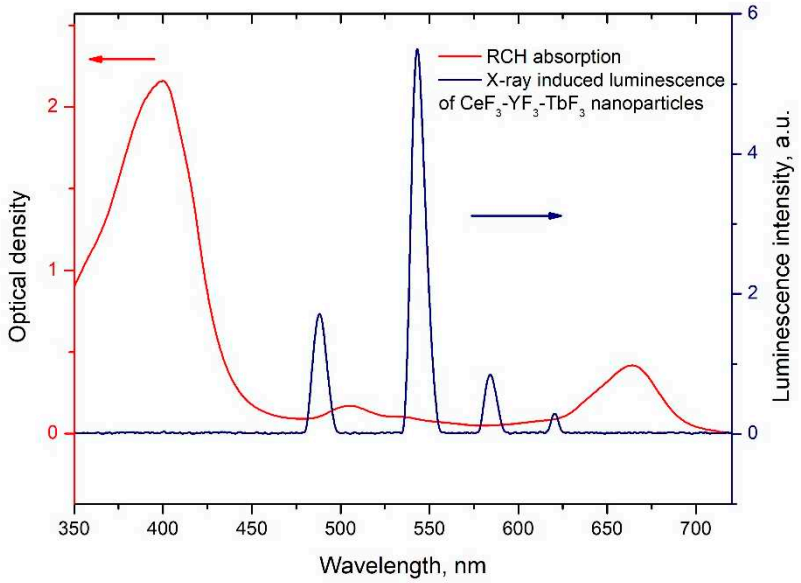

Figure 5. Radachlorin absorption spectrum and X-ray luminescence spectrum of $Ce_{0.5}Y_{0.35}Tb_{0.15}F_3$ nanoparticles.

The information concerning the spectral overlap of Radachlorin absorption spectrum and X-ray luminescence spectrum of $Ce_{0.5}Y_{0.35}Tb_{0.15}F_3$ nanoparticles allows obtaining the critical radius R_0 =4.5 nm for these conjugates [16]. Substituting the obtained efficiencies of energy transfer (k_{ET}) between the studied nanoparticles and Rch dye molecules into formula 2 [35], the distances r between them observed in the experiment were calculated . The obtained values are presented in Table 1. The absence of Ce^{3+} emission under X-ray excitation can be explained by shorter Ce^{3+} lifetime (tens of nanoseconds) compared to Tb^{3+} one (several milliseconds).

$$k_{FRET} = \frac{1}{1 + \left(\frac{r}{R_0}\right)^6} \quad (3)$$

Table 1. Distances between $Ce_{0.5}Y_{0.35}Tb_{0.15}F_3$ nanoparticles and Radachlorin molecules.

The amount of Rch, μL	distance r, nm	
	unmodified	coated with PVP
10	8.1 ± 1.2	6.3 ± 1.2
30	6.4 ± 1.2	4.6 ± 1.2
50	5.8 ± 1.2	4.2 ± 1.2
70	5.9 ± 1.2	5.0 ± 1.2
90	5.0 ± 1.2	3.7 ± 1.2
110	4.8 ± 1.2	3.6 ± 1.2
140	4.7 ± 1.2	3.5 ± 1.2
160	4.6 ± 1.2	3.5 ± 1.2
160 μl Rch + 0.5 ml H_2O	4.3 ± 1.2	3.5 ± 1.2
160 μl Rch + 1.0 ml H_2O	5.0 ± 1.2	3.5 ± 1.2

Preprints (www.preprints.org) | NOT PEER-REVIEWED | Posted: 16 November 2023 doi:10.20944/preprints202311.1050.v1

Based on the results of the calculations, it can be concluded, that with an increase in the number of Rch molecules in the colloid, the distance between nanoparticles and Rch molecules decreases. In the case of the lowest dye concentration, the distance between nanoparticles and Radachlorin molecules r = 8.1 nm, and for nanoparticles coated with PVP, r = 6.3 nm. In the case of the highest Rch concentration, the distance between nanoparticles and Radachlorin molecules r = 4.6 nm, and for nanoparticles coated with PVP, r = 3.5 nm. Further, after adding of the distilled water, the calculation of the distance between nanoparticles and Rch molecules for uncoated nanoparticles returns slightly decreased value, which can be explained by residual agglomeration processes between molecules and nanoparticles or by error of decay rate measurement. At the same time with the subsequent addition of water to coated nanoparticles this distance did not change; therefore, a stable conjugate was formed.

3.4. Evaluation of the survival of A 549 cells in the presence of $Ce_{0.5}Y_{0.35}Tb_{0.15}F_3$ nanoparticles and Radachlorin

Human lung carcinoma cells (A549) were used to assess the cytotoxicity of the nanoparticles. Cells were cultured in 25 µl DMEM medium supplemented with 10% inactivated fetal bovine serum, 2 mM glutamine, 100 U /ml penicillin, and 100 U /ml streptomycin in 5% CO_2 at 37°C in an incubator. Approximately 350 000 cells were used for the test. The expected cytotoxicity was assessed using the MTT assay. The MTT reagent was added to each well of the cell plate. The results are presented in Figures 6 and 7).

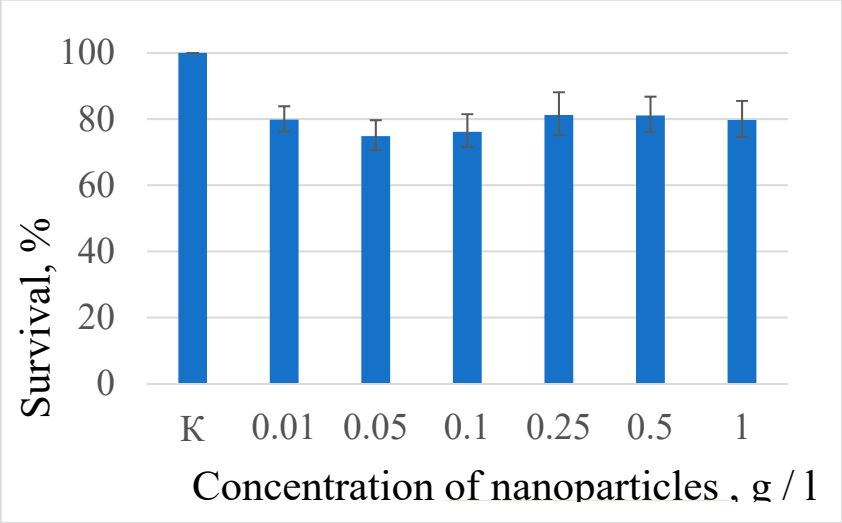

(a)

Preprints (www.preprints.org) | NOT PEER-REVIEWED | Posted: 16 November 2023 doi:10.20944/preprints202311.1050.v1

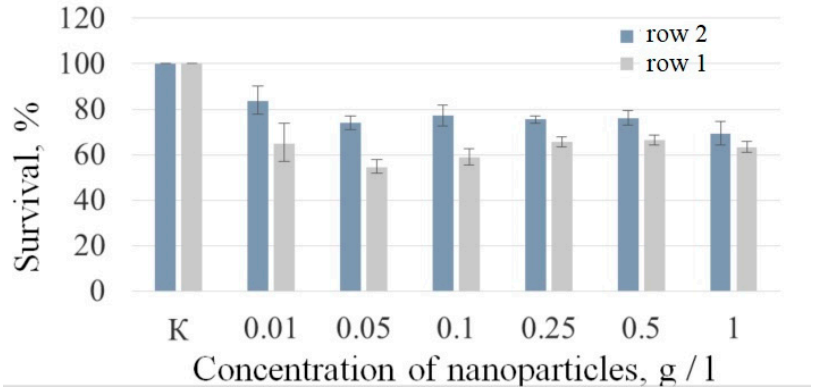

(b)

Figure 6. Cytotoxicity of $Ce_{0.5}Y_{0.35}Tb_{0.15}F_3$ unmodified nanoparticles (a) and nanoparticles coated with PVP (b) towards A549 cells. At diagram (b) row 1 - without the addition of Radachlorin; row 2 - with the addition of Radachlorin.

Figure 6a shows that there is no clear survival dependence on the nanoparticle concentration. At the same time, cell survival in the case of nanoparticles coated with PVP does not fall below 50%. An area with a high concentration is characterized by an increase in survival. It can be suggested, that for these concentrations the formation of large agglomerates takes place. These large agglomerates can precipitate without interaction with cells or this interaction (cell uptake) is hindered by the large size. It was found, that with a consistent increase in the number of Rch molecules in the colloid, the survival of A 549 cells decreases (see Figure 6b). Since the experiments were not performed in the complete darkness, the survival decrease can be explained by the generation of reactive oxygen species. Photoinduced cytotoxicity was also investigated. Cells with nanoparticles were irradiated with a laser at a wavelength of 266 nm (see Figure 7 a,b), as well as with a Latus laser device designed for photodynamic therapy using Rch (see Figures 8).

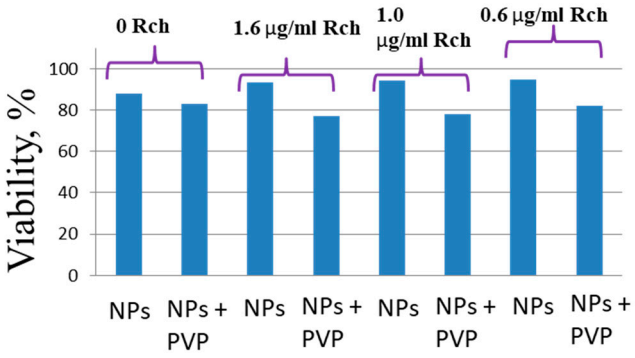

(a)

Preprints (www.preprints.org) | NOT PEER-REVIEWED | Posted: 16 November 2023 doi:10.20944/preprints202311.1050.v1

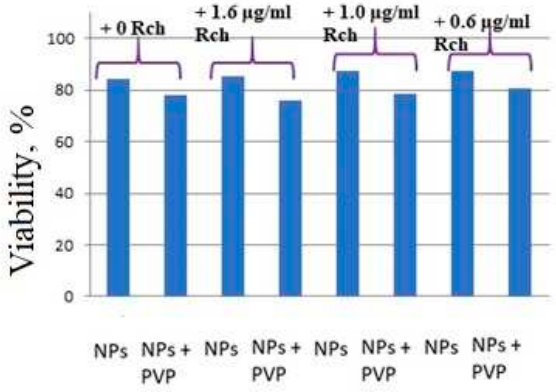

(b)

Figure 7. Photoinduced cytotoxicity of 0.1 mg/ml (a) and 0.5 mg/ ml (b) solution of $Ce_{0.5}Y_{0.35}Tb_{0.15}F_3$ nanoparticles conjugated to Rch with PVP toward A549 cells under 266 nm laser irradiation.

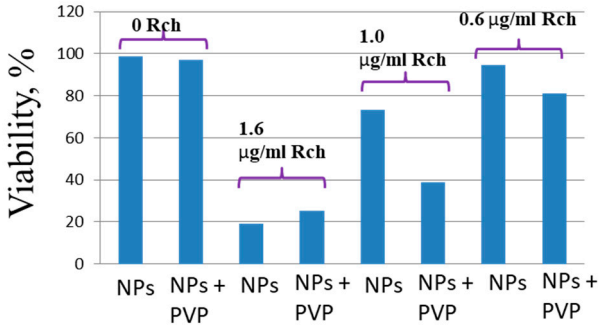

(a)

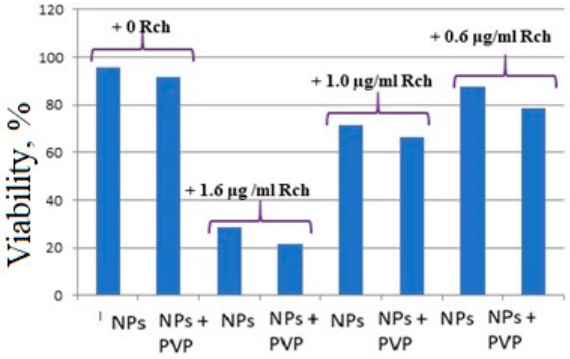

(b)

Figure 8. Photoinduced cytotoxicity of $Ce_{0.5}Y_{0.35}Tb_{0.15}F_3$ nanoparticles at a concentration of 0.1 mg/ml (a) and 0.5 mg/ml (b) conjugated to Rch using PVP on A549 cells under irradiation by Latus laser device.

It can be seem, that the photodynamic activity of both coated and unmodified nanoparticles is not significant under 266 nm irradiation. It can be suggested, that DMEM biological medium absorb

Preprints (www.preprints.org) | NOT PEER-REVIEWED | Posted: 16 November 2023 doi:10.20944/preprints202311.1050.v1

and/or scatter this kind of irradiation preventing the efficient formation of singlet oxygen. In its turn, Latus laser device provided efficient photodynamic activity of coated and unmodified samples. It can be concluded, that Rch molecules conjugated to the nanoparticles do not decompose and they are still capable of singlet oxygen generation. One of the main conclusions is, that the Rch molecule with the nanoparticle binds much better in the presence of PVP. Since nonradiative energy transfer is most efficient when the dye is conjugated with a nanoparticle, this contributes to a decrease in the survival of tumor cells. We also tested the full path of energy transfer for our scintillating nanoparticles. The cytotoxicity of the samples induced by X-ray irradiation is presented in Figure 9. The toxicity was studied towards A549 cells also. The X-ray source was presented by W-tube working at 85 kV voltages; the exposition lasted for 45 minutes.

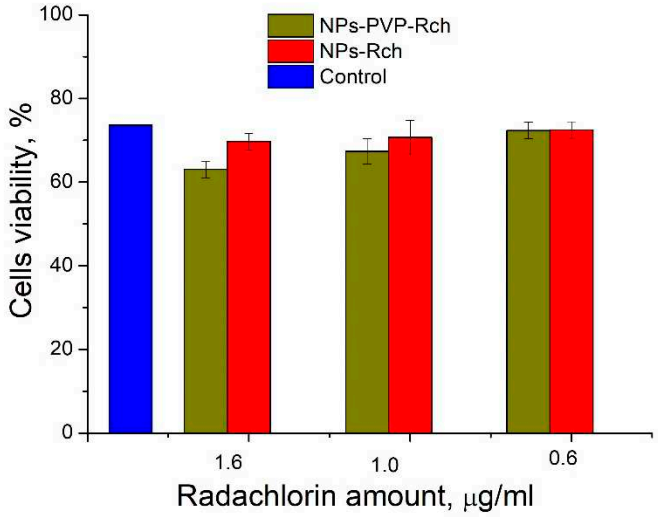

Figure 9. X-ray induced cytotoxicity of $Ce_{0.5}Y_{0.35}Tb_{0.15}F_3$ nanoparticles at a concentration of 0,1 μg/ ml conjugated to Radachlorin using polyvinylpyrrolidone on A549 cells

We can see that $Ce_{0.5}Y_{0.35}Tb_{0.15}F_3$-Rch composites do not work effectively. As it was mentioned above, that unmodified nanoparticle-Rch does not demonstrate stability (Figure 4b). In its turn, $Ce_{0.5}Y_{0.35}Tb_{0.15}F_3$-PVP-Rch composites provide notable decrease of cells viability. In particular, after X-ray irradiation the survival decreased by ~12%.

4. Conclusions

The studied $Ce_{0.5}Y_{0.35}Tb_{0.15}F_3$ nanoparticles were synthesized by co-precipitation from aqueous solution technique. All of samples had the expected CeF_3 hexagonal structure with average nanoparticle diameter around 14±1 nm. The luminescence decay curves of $Ce_{0.5}Y_{0.35}Tb_{0.15}F_3$ nanoparticles (λ_{em} = 541 nm, $^5D_4 - {}^7F_5$ transition of Tb^{3+}) conjugated with Radachlorin by means of polyvinylpyrrolidone coating as well as without Radachlorin were detected. Efficient nonradiative energy transfer from Tb^{3+} to the Radachlorin was demonstrated. The maximum energy transfer coefficient for nanoparticles conjugated with Radachlorin via polyvinylpyrrolidone was approximately 82%, and without the coating it was about 55%. Presumably, the dye molecule with the nanoparticle binds much better in the presence of polyvinylpyrrolidone. The average distance between nanoparticle surface and Radachlorin was R_0 =4.5 nm. With an increase of Radachlorin concentration led to the shortening of the distance between nanoparticles and Radachlorin. After addition of water, this distance does not change (only for PVP coated samples). It means that the conjugates are stable in our experimental conditions. The cytotoxicity of the composites was assessed using the MTT test, which revealed that with a consistent increase in the number of Radachlorin molecules in the colloid, the survival of A549 cells declines. The best results for X-ray induced cytotoxicity was observed for NP-PVP-Rch sample at the lowest Rch concentration. In particular, after X-ray irradiation the survival decreased by 12%.

Supplementary Materials: Not applicable.

Author Contributions: conceptualization: A.N., investigation: A.K., A.N., N.Sh, S.K., D.S., E.L., M.G., S.B., S.K., S.Z., P.Z., and M.P. data curation: A.K., A.N., N.Sh, S.K., E.L., M.G., P.Z., and M.P., writing—original draft preparation: A.K., A.N., S.K., and M.P., writing—review and editing: A.N., and M.P., project administration A.N., and M.P, funding acquisition: A.N., and M.P.

Funding: This research was funded by the subsidy allocated to Kazan Federal University for the state assignment in the sphere of scientific activities (project number FZSM-2022-0021).

Institutional Review Board Statement: Not applicable.

Informed Consent Statement: Not applicable.

Data Availability Statement: Not applicable.

Conflicts of Interest: The authors declare no conflict of interest.

References

1. Algorri, J. F., Ochoa, M., Roldán-Varona, P., Rodríguez-Cobo, L., López-Higuera, J. M. Photodynamic therapy: A compendium of latest reviews. *Cancers*, 2021, *13*(17), 4447.
2. Correia, J. H., Rodrigues, J. A., Pimenta, S., Dong, T., Yang, Z. Photodynamic therapy review: principles, photosensitizers, applications, and future directions. *Pharmaceutics*, 2021, *13*(9), 1332.
3. Kustov, D. M., Kozlikina, E. I., Efendiev, K. T., Loshchenov, M. V., Grachev, P. V., Maklygina, Y. S., Loschenov, V. B. Laser-induced fluorescent visualization and photodynamic therapy in surgical treatment of glial brain tumors. *Biomedical Optics Express*, 2021, *12*(3), 1761-1773.
4. Kustov, A. V., Smirnova, N. L., Privalov, O. A., Moryganova, T. M., Strelnikov, A. I., Morshnev, P. K., Berezin, D. B. Transurethral resection of non-muscle invasive bladder tumors combined with fluorescence diagnosis and photodynamic therapy with chlorin e6-type photosensitizers. *Journal of Clinical Medicine*, 2021, *11*(1), 233.
5. Hemmer, E., Benayas, A., Légaré, F., & Vetrone, F. Exploiting the biological windows: current perspectives on fluorescent bioprobes emitting above 1000 nm. *Nanoscale Horizons*, 2016, *1*(3), 168-184.
6. Bashkatov, A. N., Genina, E. A., & Tuchin, V. V. Optical properties of skin, subcutaneous, and muscle tissues: a review. *Journal of Innovative Optical Health Sciences*, 2011, *4*(01), 9-38.
7. Ginner, L., Gesperger, J., Wöhrer, A., Drexler, W., Baumann, B., Leitgeb, R., Niederleithner, M. Ex-vivo Alzheimer´ s disease brain tissue investigation: a multiscale approach using 1060-nm swept source optical coherence tomography for a direct correlation to histology. *Neurophotonics*, 2020, 1-12.
8. Pudovkin, M. S., Zelenikhin, P. V., Krasheninnikova, A. O., Korableva, S. L., Nizamutdinov, A. S., Alakshin, E. M., Kadirov, M. K. Photoinduced toxicity of PrF3 and LaF3 nanoparticles. *Optics and Spectroscopy*, 2016, *121*, 538-543.
9. Pudovkin, M. S., Zelenikhin, P. V., Shtyreva, V. V., Evtugyn, V. G., Salnikov, V. V., Nizamutdinov, A. S., Semashko, V. V. Cellular uptake and cytotoxicity of unmodified Pr 3+: LaF3 nanoparticles. *Journal of Nanoparticle Research*, 2019, *21*, 1-13.
10. Pudovkin, M. S., Korableva, S. L., Krasheninnicova, A. O., Nizamutdinov, A. S., Semashko, V. V., Zelenihin, P. V., Nevzorova, T. A. Toxicity of laser irradiated photoactive fluoride PrF3 nanoparticles toward bacteria. In *Journal of Physics: Conference Series* , 2014, 560, 1, 012011.
11. J. Yu *et al.*, Biodistribution, excretion, and toxicity of polyethyleneimine modified NaYF4:Yb,Er upconversion nanoparticles in mice via different administration routes, *Nanoscale*, 2017, 9, 13, 4497–4507.
12. Li, H., Wei, M., Lv, X., Hu, Y., Shao, J., Song, X., Dong, X. Cerium-based nanoparticles for cancer photodynamic therapy. *Journal of Innovative Optical Health Sciences*, 2022, *15*(06), 2230009.
13. Ca, N. X., Vinh, N. D., Bharti, S., Tan, P. M., Hien, N. T., Hoa, V. X., . Do, P. V. Optical properties of Ce3+ and Tb3+ co-doped ZnS quantum dots. *Journal of Alloys and Compounds*, 2021, *883*, 160764.
14. Akman, P., Ulusan, S., Banerjee, S., Yilmaz, A. Core/shell type, Ce3+ and Tb3+ doped GdBO3 system: Synthesis and Celecoxib drug delivery application. *Microporous and Mesoporous Materials*, 2020, *308*, 110528.

15. Nizamutdinov, A. S., Madirov, E. I., Lukinova, E. V., Kiyamov, A. G., Andreeva, D. D., Pudovkin, M. S., Semashko, V. V. (2020). Spectral-Kinetic Properties and Energy Transfer in Nanoparticles of Y 0.5–x Ce 0.5 Tb x F 3 Solid Solution. *Journal of Applied Spectroscopy*, 2020, *87*, 481-487.
16. Nizamutdinov, A., Lukinova, E., Shamsutdinov, N., Zelenikhin, P., Khusainova, A., Gafurov, M., Pudovkin, M. CeF3-YF3-TbF3 Nanoparticle-Polymer–"Radachlorin" Conjugates for Combined Photodynamic Therapy: Synthesis, Characterization, and Biological Activity. *Journal of Composites Science*, 2023, *7*(6), 255.
17. Rimoldi, T., Orsi, D., Lagonegro, P., Ghezzi, B., Galli, C., Rossi, F., Cristofolini, L. CeF 3-ZnO scintillating nanocomposite for self-lighted photodynamic therapy of cancer. *Journal of Materials Science: Materials in Medicine*, 2016, *27*, 1-9.
18. Orsi, D., Rimoldi, T., Pinelli, S., Alinovi, R., Goldoni, M., Benecchi, G., Cristofolini, L. New CeF3–ZnO nanocomposites for self-lighted photodynamic therapy that block adenocarcinoma cell life cycle. *Nanomedicine*, 2018, *13*(18), 2311-2326.
19. Ahmadi, H., Bagherzadeh, M., Raeisi, M., Payami, F. Preparation and characterization and photoluminescence properties of CeF 3@ ZnS nanocomposites. *Journal of Materials Science: Materials in Electronics*, 2020, *31*, 3215-3220.
20. Xiang, H., Xue, F., Yi, T., Tham, H. P., Liu, J. G., Zhao, Y. Cu2–x S Nanocrystals Cross-Linked with Chlorin e6-Functionalized Polyethylenimine for Synergistic Photodynamic and Photothermal Therapy of Cancer. *ACS applied materials & interfaces*, 2018, *10*(19), 16344-16351.
21. Zhiyentayev, T. M., Boltaev, U. T., Solov'eva, A. B., Aksenova, N. A., Glagolev, N. N., Chernjak, A. V., Melik-Nubarov, N. S. Complexes of chlorin e6 with pluronics and polyvinylpyrrolidone: structure and photodynamic activity in cell culture. *Photochemistry and Photobiology*, 2014, *90*(1), 171-182.
22. Hädener, M., Gjuroski, I., Furrer, J., Vermathen, M. Interactions of polyvinylpyrrolidone with chlorin e6-based photosensitizers studied by NMR and electronic absorption spectroscopy. *The Journal of Physical Chemistry B*, 2015, *119*(36), 12117-12128.
23. Solov'eva, A. B., Khasanova, O. V., Aksenova, N. A., Chernyak, A. V., Volkov, V. I., Timofeeva, V. A., Timashev, P. S. The Influence of Effect of Polysaccharides and Polyvinylpyrrolidone on the Photocatalytic Activity of Chlorin e6 in Tryptophan Oxidation. *Russian Journal of Physical Chemistry A*, 2019, *93*, 2507-2514.
24. Tsvetkov, V. B., Solov'eva, A. B., & Melik-Nubarov, N. S. Computer modeling of the complexes of Chlorin e6 with amphiphilic polymers. *Physical Chemistry Chemical Physics*, 2014, *16*(22), 10903-10913.
25. Gadzhimagomedova, Z., Polyakov, V., Pankin, I., Butova, V., Kirsanova, D., Soldatov, M., Soldatov, A. BaGdF5 Nanophosphors Doped with Different Concentrations of Eu3+ for Application in X-ray Photodynamic Therapy. *International Journal of Molecular Sciences*, 2021, *22*(23), 13040.
26. Alakshin, E. M., Klochkov, A. V., Kondratyeva, E. I., Korableva, S. L., Kiiamov, A. G., Nuzhina, D. S., . Kodjikian, S. Microwave-assisted hydrothermal synthesis and annealing of DyF3 nanoparticles. *Journal of Nanomaterials*, 2016, *2016*.
27. Wang, X., Sheng, T., Fu, Z., Li, W. Highly uniform YF3: Ln 3+ (Ln= Ce 3+, Tb3+) walnut-like microcrystals: Hydrothermal synthesis and luminescent properties. *Materials Research Bulletin*, 2013, *48*(6).
28. Bekah, D., Cooper, D., Kudinov, K., Hill, C., Seuntjens, J., Bradforth, S., Nadeau, J. Synthesis and characterization of biologically stable, doped LaF3 nanoparticles co-conjugated to PEG and photosensitizers. *Journal of Photochemistry and Photobiology A: Chemistry*, 2016, *329*, 26-34.
29. Efendiev, K. T., Alekseeva, P. M., Shiryaev, A. A., Skobeltsin, A. S., Solonina, I. L., Fatyanova, A. S., Loschenov, V. B. Preliminary low-dose photodynamic exposure to skin cancer with chlorin e6 photosensitizer. *Photodiagnosis and Photodynamic Therapy*, 2022, *38*, 102894.
30. Camus-Génot, V., Lhoste, J., Moury, R., Galven, C., Hémon-Ribaud, A., Pascual, S., Guiet, A. Facile preparation of 3D interconnected macroporous CeF3. *Journal of Solid State Chemistry*, 2023, *324*, 124099.
31. Pudovkin, M. S., Ginkel, A. K., Morozov, O. A., Kiiamov, A. G., Kuznetsov, M. D. Highly-sensitive lifetime optical thermometers based on Nd3+, Yb3+: YF3 phosphors. *Journal of Luminescence*, 2022, *249*, 119037..
32. Guo, B., Zhang, Z. W., Jiang, D. G., Li, Y. N., Sun, X. Y. Generation of bright white-light by energy-transfer strategy in Ca19Zn2 (PO4) 14: Ce3+, Tb3+, Mn2+ phosphors. *Journal of Luminescence*, 2019, *206*, 244-249.
33. Sahoo, H. Förster resonance energy transfer–A spectroscopic nanoruler: Principle and applications. *Journal of Photochemistry and Photobiology C: Photochemistry Reviews*, 2011, *12*(1), 20-30.

34. Clegg, R. M. Förster resonance energy transfer—FRET what is it, why do it, and how it's done. *Laboratory techniques in biochemistry and molecular biology*, 2019, *33*, 1-57.
35. Li, X., Zhang, W., Dong, L., Liu, D., Qi, Z.. Low temperature molten salt synthesis of CeF3 and CeF3: Tb3+ phosphors with efficient luminescence properties. *Journal of Luminescence*, 2019, *205*, 122-128.